Polypropylene fiber reinforced cement mortars containing rice husk ash and nano-alumina

Ehsan Mohseni[1*], Mojdeh Mehrinejad Khotbehsara[1], Farzad Naseri[2], Maryam Monazami[3] and Prabir Sarker[4]

[1] Department of Civil Engineering, University of Guilan, Rasht, Iran

[2] Department of Civil Engineering, Islamic Azad University-East Tehran Branch, Tehran, Iran

[3] Department of Civil Engineering, University of Shahrood, Shahrood, Iran

[4] Department of Civil Engineering, Curtin University, Perth, Australia

[*]*Corresponding Author: Mohseni@msc.guilan.ac.ir;*
Ehsan.mohseni172@gmail.com
Tel: +98 9125590423

Abstract

This paper presents the effects of incorporating two supplementary cementitious materials: rice husk ash (RHA) and nano-Alumina (NA) in polypropylene fiber (PPF) reinforced cement mortars. RHA is an agricultural waste material and thus recycling of this material has substantial economic and environmental benefits. Compressive strength, flexural strength, water absorption and drying shrinkage of the hardened composites were investigated. The interfacial transition zone and the microstructures were studied by using Scanning Electron Micrograph (SEM) and X-ray Diffraction (XRD) analysis. A slight increase in compressive strength of mortar was observed by using up to 10wt% of RHA as a replacement of cement. However, addition of nano-Alumina helped the compressive strength of mortar remain approximately equal to that of the control specimen even when 20 or 30wt% RHA was used. Addition of polypropylene fibers resulted in significant increase in the flexural strength of the mortar specimens. It was also observed that NA and PPF could reduce water absorption by pore blocking effect. The positive interactions between polypropylene fibers and RHA resulted in the lowest drying shrinkage of the fibrous mortar containing RHA. XRD analysis showed that the intensity of Alite and Belite phases decreased and new peak of portlandite produced with the addition of NA. The addition of RHA enhanced the late strength of the cement composites. Consequently, the combined addition of RHA, NA and PPF has resulted in increasing of flexural strength and reduction in both water absorption and drying shrinkage of SCMs.

Key words: Polypropylene fiber; Rice husk ash; Nano-Al_2O_3; Compressive and flexural strength; Water absorption; Drying shrinkage.

1. Introduction

Concrete can be made greener by using waste materials that reduce its environmental impact such as the reduction of CO_2 emission in cement production. According to the European Cement Association, the concrete technology today allows for new buildings to be built with 60% less energy use and CO_2 emissions over the lifecycle of the building than conventional buildings constructed 20 years ago [1]. In the mix design, there are also extra steps taken to improve the sustainability of a structure with a long life cycle. Fly ash, blast furnace slag, recycled concrete, power plant waste, rice husk ash, waste glass, red mud, burnt clay, etc. are some of the waste materials used in concrete. Rice husk ash (RHA) is a carbon neutral green product and several ways are currently being used for disposing them [2-4]. Annually a large amount of rice is produced in the rural areas of different countries such as Iran, Malaysia, Thailand, Bangladesh, India, Pakistan, Myanmar etc. Huge quantities of rice husk are produced during the processing of this rice. The rice husk is used as fuel which generates the rice husk ash. Incorporating rice husk ash in concrete as a cement replacement has many environmental and economic advantages. RHA is a good pozzolan that can be used to make concrete. Using rice husk ash in concrete has been examined by many researchers around the world. The initial and important reviews on the use of RHA in concrete focused on the mechanical performance of concrete [2-9]. However, recent studies have mostly worked on the concrete properties when RHA with additional admixtures were incorporated [10-14]. Using wood fiber waste (WFW), rice husk ash (RHA), and limestone powder waste (LPW) as cement replacement materials in lightweight concrete blocks was studied by Torkaman et al. in 2013 [10]. The results indicated that the bulk density and water absorption of concrete samples were significantly reduced by the addition of RHA. Sharma [11] reported that up to 10% mass of cement can be replaced by RHA that is mixed with plastic fibers with nearly equivalent compressive strength.

RHA was incorporated in different types of concrete such as normal concrete, self-consolidating concrete and high performance concrete [12-18]. Madandoust [12] reported that the use of 20wt% RHA in normal concrete reduced the early-age strength development. Safiuddin et al. [13] investigated the flowing ability of self-consolidating concrete and its binder paste and mortar components with rice husk ash. The results showed good improvement in the flow ability of the mixtures when the rice husk ash was added to the binder. The test results revealed that the w/b ratio and RHA content significantly influenced the flowing abilities of the binder pastes, mortars and concretes. However, using RHA may also decrease the flowing ability

of the self-compacting concretes. In another study, Safiuddin et al. [14] showed that the flowing ability of mortar mixtures decreased as the amount of RHA was increased. Robler et al. [15] reported that due to the mesoporous structure of RHA, it absorbs free water, so the w/b ratio in the cementitious matrix is reduced and the compressive strength is increased consequently.

Nanoparticles have been recently used as a cement replacement to tailor the mechanical properties of concrete [19-24]. These particles increase the cement hydration and act as a filler to reduce the porosity of mortar. Noorvand et al. [20] examined the effect of nano-TiO_2 in black rice husk ash concrete. The results showed improvement in both mechanical and micro-structural properties of mortars with black rice husk ash. In their study, the compressive strength was found to increase by up to 18% when black rice husk ash and nanoparticles were used in the mortar. However, the compressive strength decreased by about 27% when black rice husk ash was used singly.

Polypropylene fiber (PPF) was incorporated in concrete for many years to enhance the flexural properties and also restrain the progression of cracks [25-31]. It also improves the strength of concrete against impacts and fatigue. Medina [30] reported that the cracking control ability of PPF on the exposed concrete surface reduced water permeability and CO_2 diffusion. It also increased porosity and reduced bulk density and the ultrasonic modulus of natural pozzolan cement concretes.

The ingress of various ions from the environment and its movement through building materials are the main reasons for deterioration of structures. So, the control of the permeability of concrete plays an important role in providing resistance to aggressive environment [32]. In this study, a novel combination of nano-alumina (NA), RHA and PPF was used in concrete. The aim was to partially replace Portland cement by RHA and make mixtures of improved properties in hardened stages by the addition of NA and PPF.

2. Experimental program

2.1 Materials

Natural river sand and ordinary Portland cement type I conforming to ASTM C778 [33] and ASTM C150 [34], respectively were used. According to the ASTM standard, rice husk ash (RHA) can be used as a pozzolanic material with cement [35]. The particle size distribution curve of RHA is given in Fig. 1. The physical properties of RHA substantially depend on the burning conditions. Particularly, the temperature and period of burning influence on the microstructure and crystallinity of RHA [36]. The partial burning of rice husks produces black RHA whereas the

complete burning results in either white or gray RHA. Hwang & Chandra [37] suggested that burning rice husk at temperatures below 700°C provides amorphous silica. In this study the husk was sourced from Rasht, Iran and an electric kiln was used to burn the rice husk pellets. Heating cycles were conducted by an electric system with a heating rate of 5°C/min. Each sample was held at temperatures between 500 and 700°C for 6 hours. The XRD results illustrate that when the RHA was burned within 300°C to 700°C, it turned into amorphous silica. For instance, the XRD pattern of the ash indicates the presence of noncrystalline silica as seen in Fig. 2. RHA is mainly composed of silica, which constitutes 91% of the total mass. This amount of silica is seen as Quartz in XRD diagram of RHA. The chemical composition and physical properties of cement and RHA are given in Table 1. Nano-Al_2O_3 in dispersed suspension form with an average particle size of 20 nm, specific surface area of 200m^2/g and purity of higher than 98% was used in this study. Fig. 2-a and 2-b show the XRD diagrams of the nano-Al_2O_3 and RHA. The scanning electron micrographs (SEM) of nano-Al_2O_3 and RHA are given in Fig. 3. It can be seen from these figures that nano-Al_2O_3 particles are spherical while the RHA particles are of irregular shape. In order to achieve the desired fluidity and better dispersion of the nanoparticles, a polycarboxylate type superplasticizer (SP) conforming to ASTM C494 [38] with a density of 1.03 g/cm^3 was utilized. The content of superplasticizer was adjusted for each mixture to keep the slump flow of mortars 25±1 cm.

Polypropylene fibers (PPF) produced from recycled raw materials was chosen because of its high resistance to corrosion and chemical leaching, its resilience against impact and freezing, and its environmental benefits. A photograph of the fibres is shown in Fig. 4 and the properties of the fibres are given in Table 2. The fibres with a length of 6 mm and a diameter of 20 micron making an aspect ratio of 300 was utilized at a dosage of 0.3% by volume.

2.2 Mix proportions

Twenty six mixtures were prepared with different amounts of RHA, NA, PPF and SP. The percentage of RHA was varied between 0 and 30% by weight of the total binder. The percentage of nanoparticles was 0, 1, 2 and 3%, and PPF was used in 0 and 0.3% of the binder. The amount of SP varied between 0.2 and 1% by weight of the binder. The water to binder ratio (w/b) was kept constant at 0.49 for all mixtures. Detailed mix proportions of the mortars are given in Table 3. In labeling of the mixtures, the number after RHA, NA and PPF represents the percentage of rice husk ash, Nano-Alumina and Polypropylene fibres respectively.

2.3 Production of specimens

Nanoparticles may not always show a uniform distribution in the mixture due to their large surface area [39]. As this could directly affect the physical and

mechanical properties of the mortars, the specimen production procedure used in this study was carried out in accordance with the ASTMC305 standard [40]. However, some change in the mixing procedure was necessary due to presence of nanoparticles. Masks and gloves were used to avoid direct contact with the fine particles during the mixing. First, the cement and RHA were dry mixed in the mixer at a moderate speed (80rpm) for 1 min. Then, these components were mixed at a high speed (120rpm) for 90 seconds with the nanoparticles, 90% of the water and the specified amount of fibers. The sand was then gradually added over a period of 30 seconds while the mixer was running at a moderate speed (80rpm). Eventually the superplastisizer and remaining water were added and stirred at high speed (120rpm) for 30 seconds. After this, the mixture was allowed to rest for 90 seconds and then mixing was continued for 1 minute at a high speed (120rpm). This mixing procedure was followed to facilitate the distribution of the nanoparticles and the fibers in the mortar.

Fresh mortar was cast into 50×50×50 mm cubes for compressive strength and water absorption tests and in 50×50×200 mm steel moulds for flexural and shrinkage tests. The specimens were compacted using a tamping rod to exclude the air bubbles from the mortar. The specimens were demolded 24 hours after casting and cured in water at 23±3 °C until they were tested.

2.3 Test procedure

Compressive strength test was conducted in accordance with the ASTM-C109 standard [41] using a hydraulic testing machine at a loading rate of 1350N/s. The three-point (i.e. center-point) loading flexural test was carried out with the span of 180mm and at a loading rate of 44N/s. The compressive and flexural strength results were determined at 28 and 90 days of curing. The average value of the test results of three specimens was reported.

The water absorption test was carried out at 28 days of age. Saturated surface dry specimens were kept in an oven at 110℃ for 72 hours. After determination of the initial weight, the specimens were immersed in water for 72 hours. The final weight was then determined and the absorption was calculated to assess the permeability of the mortar specimens. The absorption value was obtained by taking an average of the test results of two specimens.

To determine the drying shrinkage, (50×50×200) mm prisms were tested in accordance with ASTM C157-89 [42]. Two gauge studs were inserted at the two ends (along the center axis) of each specimen immediately after casting of the specimens. The specimens were demoulded 24 hours later and placed in water for 7 days. After this the specimens were removed from water and the initial dial gauge readings were taken immediately. Then the specimens were stored in dry room of the laboratory with temperature of 23±2℃ and a relative humidity of 50±4%. The

length change tests were taken at ages (7, 28, 60 and 90) days. The length change of specimens was measured by means of a length comparator conforming to the requirement of ASTM C490-00a [43]. The specimen was rotated slowly in the measuring device, while the measurement of length was being made. The accuracy of the dial gauge of the measuring device was 0.002 mm. The average value of four readings from two prisms was adopted for each mix.

3. Results and discussion

3.1. Compressive strength

The compressive strength values of mortar specimens are given in Table 4 and the variations of strength with age are plotted in Fig. 5. The results show a slight increase in compressive strength by the addition of RHA up to 10wt% and a reduction in strength with further increase in the RHA content. The improvement in the strength of mortars incorporating RHA, especially at later ages is due to its pozzolanic action. The calcium silicate hydrate (CSH) gel produced by the reaction of the high silica content of RHA with the $Ca(OH)_2$ generated from the hydration of cement contributes to the continued increase of strength at the later ages. Similar effect of RHA was also observed in previous works [12]. Giaccio et al. [44] showed in the experiments that incorporating RHA as 10wt% of the binder improved the compressive strength of concrete samples. Gastaldini et al. [45] also reported enhancement in compressive strength, when RHA was used as partial replacement of cement. However, excessive amounts of RHA could decrease the compressive strength. Figs. 6-a, 6-b and 6-c show the SEM images of control specimen, a specimen with 10%RHA, and a specimen with 10%RHA and 3%NA, respectively. The solid phase of mortar is composed of 5 parts: C-S-H, C-H, ettringite, monosulfate and residual unhydrated cement. These 5 parts are different in their volume fraction, density, dimensions, morphology and Christianity. So characterization is usually done by SEM micrograph, especially for understanding the morphology and dimensions of solid parts. Unreacted materials are materials that do not resemble to any products of the hydration. The black spaces in SEM photos are the capillary pores which are decreased, when nano- alumina is added. As a definition, capillary pore is the space which is not taken up by the cement and hydration products (dependent on w/c); 2.5-50nm in size in well-hydrated concrete. These pores are irregular in shape, also size and amount are related to w/c and degree of hydration. Micropores with diameter less than 50 nm are more crucial for drying shrinkage and creep and macropores with diameter more than 50 nm are more significant for strength. As it is seen in Fig. 6-b, the amount of pores is reduced by the addition of RHA in comparison with that of the specimen without RHA as shown in Fig. 6-a. However, couple of unreacted particles can be clearly seen in Fig. 6-b.

Using nanoparticles fostered the compressive strength of specimens substantially. The effect of nanoparticles in mortars can be summarized in the following 3 steps:

1. Nano-Alumina works as fillers to fill the pores, so the compactness of samples is enhanced [46]. As it can be seen in SEM images of the specimen with RHA and NA in Fig. 6-c, there are fewer and smaller pores and the microstructure is more compacted when NA is added. This is due to the fact that nanoparticles are expected to affect the kinetics and hydration of cement substantially and yield greater filling of voids of cement-based composites in comparison with the mineral additives in virtue of their larger surface area and greater electrostatic force.

2. Hydration of cement is a sum of chemical reactions between cement and water. A third type of material may affect the hydration process. High specific surface of nano-alumina particles accelerates the hydration process by rapid dissolution of cementitious compounds. This led to the formation of clusters of calcium aluminosilicate (C-A-S-H) gel.

3. Nanoparticles make the cement matrix homogenous and makes the structure compacted. As it is shown in Fig. 6-c, there are less unhydrated cement and more homogenous cement matrix in comparison with the control sample.

Table 4 also shows that when the amount of RHA is 30%, using NA more than 2 % has an inverse effect and decreases the compressive strength. When a mixture contains 30% RHA, for the rest of 70% cement, homogeneous hydrated microstructure cannot be formed, because the nanoparticles cannot be well dispersed. By addition of excessive amount of nanoparticles, they replace part of the cementitious materials, nonetheless this does not affect the strength and the excess silica will leach out and cause a deficiency in strength. Dispersion of nanoparticles is the main reason of the formation of homogeneous structure that is an important factor in compressive strength of a specimen. So despite the best result was achieved when 3% NA was used, using 2% NA gives the best average mechanical and economical results.

As expected, the results also show that addition of PPF did not have a significant effect on the compressive strength of samples. Also in some specimens like RHA20NA3 addition of PP decreases the compressive strength slightly. According to the Table 5, RHA10NA3PP0.3 showed the best result, as the increase percentage was 18.2 and 20.1 at 28 and 90 days respectively.

Also the outstanding impact of age on improvement of compressive strength can be seen in Table 4. In all samples, percentage of decrease was lowered or the percentage of increase was heightened, when the curing time increased from 28 days to 90 days. In the mixtures with RHA, the amount of cement is lower than in the control sample. So at the early ages, the structure was less compact and the volume

of pores increased as the amount of RHA increased. As the age of curing increased, the pozzolanic reactions increased that caused a higher density of the product. Presence of nanoparticles was the other way of filling the pores when RHA is incorporated. The similar comparison was also reported by Chao-Lung et al. [47]. The results are similar between early age and 28 days of curing. As a result, the process of improving compressive strength and the pozzolanic reactions are started at early ages and continued at least up to the age of 90 days.

3.2. Flexural strength

The flexural strength results are presented in Table 5, while the variation of flexural strength with time is shown in Fig. 7. The results indicate the outstanding effect of adding PPF in the improvement of flexural strength. It can be seen that the mixes with PPF and RHA showed higher values in comparison with that of the control sample. Also, flexural strength of specimens incorporating nanoparticles in most cases was higher than that of the control sample. However, these particles strengthen the weak region that is between cement paste and RHA. The SEM images of specimens incorporating RHA, NA and PPF, which are given in Figs. 9-a and 9-b, confirm this statement. The nanoparticles fill the pores especially porous portlandite crystals which array in the interfacial transition zone (ITZ) between cement matrix and RHA.

It can be seen in Table 4 that the addition of 30wt% RHA lowered the flexural strength up to about 14%. Instead the addition of 0.3% PPF boosted flexural strength up to 14%, which was equal to the value for the control sample. By comparison of Fig. 6-b and Fig. 8-a, it is evident that using PPF can balance out the negative effects of RHA incorporation. As it is shown, PPF in mortars look like very small bars that can control the crack propagation.

The results also show that when the amount of RHA is 30%, adding nanoparticles more than 2% lowers the flexural strength by about 1.5%. This result was also obtained in compressive strength test. The effect of aging on improvement of flexural strength is also evident. In all samples the percentage decrease was improved when specimens were tested after 90 days of curing.

It is verified that specimens that were not reinforced with PPF exhibited brittle failure. These failures started with micro cracks in the cement-aggregate interface that then propagated as the load increased. The PPF reinforced specimens, however, exhibited ductile failure. The initial cracks started in the cement matrix, but they did not propagate as fast as in the case of plain mortar specimens. This is due to the reinforcing ability of PPF to limit cracking from its unique high strength bond with the cementitious materials. Microscopic analysis of mortar fracture surface (Fig. 9a and 9b) shows that micro cracks exist at the aggregate-matrix interface of the plain mortar specimen even before any load has been applied to the mortar. The formation

of such cracks is due primarily to the strain and stress concentrations resulting from the incompatibility of the elastic moduli of the aggregate and paste components. On the other hand, the strong bond between the fibers and cement paste in the PPF reinforced mortar specimen reduces such cracks (Fig. 9c). The composite system of mortar reinforced with PPF is assumed to work as if it were unreinforced until it reaches its ‘‘first crack strength.” It is from this point that the reinforcing fibers take over and hold the mortar together.

Typical flexural load displacement response of different mixtures containing 0.3% PPF and 3% nano-Al_2O_3 at 90 days are represented in Fig. 10. The test was controlled automatically by computer with a constant cross head movement of 1mm/min. As it is evident, unreinforced mortar demonstrated brittle behavior. The samples fully fractured with the increase of mid span displacement after peak load, while fiber reinforced mortar exhibited ductile behavior. Study of the load-displacement curve showed that mortar containing nano-Al_2O_3 was obviously more brittle than that of control mortar, however, integrating PP fibers somewhat compensated this shortage. A relatively big increase was observed when increasing the PPF content to 0.3%. When cracks occurred and propagated, the fibers were able to bridge across the cracks, preventing the crack-face separation. The fibers sustained the load until they pulled out from the matrix. This mechanism provides an additional energy absorption which led to a stable fracture process and higher fracture energy. The presence of nano-Al_2O_3 enhanced the efficiency of the transfer of load from matrix to fiber by increasing the friction coefficient between the fiber and the matrix. Hence the sample containing PP fibers and nano-Al_2O_3 showed a higher peak-load with long post-peak curve as compared to the other samples, as shown in Fig. 10. When enough PPF is distributed in the matrix to bridge any growing micro crack, the additional energy is consumed in breaking or pulling out the fibers, hence, leading to higher failure load and toughness to the material.

3.3 Water absorption test

Water absorption of concrete is a measure of the capillary forces exerted by the pore structure that causes fluids to be drawn into the body of the materials [48].

The experimentally obtained results are presented in Fig. 11. Each of them is the mean value of three samples tested at 28 days of curing. In general, the results showed small reductions in the absorption values when RHA was added.

Using fine particles such as RHA leads to the segmentation of large pores and fosters nucleation sites for precipitation of hydration products in cement paste. However, the replacement of cement by RHA up to 10% also reduced the water absorption of specimens. Addition of RHA more than 10% leads to an increment of water absorption. The increase in water absorption in samples with a relatively high content of pozzolans is associated with the decrease of ordinary Portland cement,

which reduces the hydration products in specimens. As shown in Fig. 6, it was observed that the incorporation of RHA in mortars could lead to extensive pore refinement in both the matrix and the interfacial zones. The resulting pore refinement can effectively decrease the water permeability.

However increase in the amount of nano-Alumina and also PPF further reduced the water absorption. Due to very high specific surface area, the nanoparticles contained some free water on the surface, which resulted in continuous hydration that made the matrix more compacted. This seems like that external curing time for mortar samples. The percentage of water absorption is related to the porosity of the hardened mortar which is engaged by water in a saturated state [5].

3.4 Drying shrinkage

Fig. 12 shows the variations of drying shrinkage over time for mortars made with different percentages of RHA and PPF. The drying shrinkage of mortars is highly related to the stiffness of aggregates and their porosity. As seen from the figure, both RHA and PPF reduced the drying shrinkage of the mortar mixtures. All the specimens started to shrink gradually after removal from water. This is in virtue of the modification of pore size distribution and the interfaces beside the rapid loss of moisture from the surface of the specimens having high cement content. The results show that drying shrinkage values increased with time and the rate decreased after about 10 weeks of age. The drying shrinkage of the mortars with RHA after 90 days ranged from 801 to 843 microstrains. Mortars made with RHA exhibited lower drying shrinkage after 90 days compared with that of the control specimen. Drying shrinkage (after 90 days) decreased by 5% to 12% when RHA increased from 10% to 30%. The variation in shrinkage with water content may be introduced by the difference in types of water lost at a wide range of stages of drying. It is also associated with the modulus of elasticity of the sample. Mortar with high water content has a lower strength and lower modulus of elasticity and hence has a greater tendency to shrinkage. Due to the higher surface area of RHA in comparison with cement, such fine particles (RHA) can absorb more water, which leads to reduction of water content and consequently the drying shrinkage is reduced. On the other hand, incorporating PPF also reduced the drying shrinkage of mortars. At 90 days, the drying shrinkage values were 729, 680, 651 and 622 microstrains for mixtures PP0.3, RHA10PP0.3, RHA20PP0.3 and RHA30PP0.3, respectively. Malhotra et al. [49] concluded that polypropylene fiber reinforced high volume fly ash concrete has very low drying shrinkage property. Liu et al. [50] and Salih and Al-Azaawee [51] stated that polypropylene fiber mixed into cement mortar decreased its dry-shrinkage. They concluded that the reduction in drying shrinkage increased with the increasing volume fraction of fibers. Kırca and Sahin [52] supported this finding and reported that the use of polypropylene fibres restrained the movements in micro level by bridging and stitching the fine cracks. This is attributed to the ability of

polypropylene fibers to minimize the density of cracks, crack length and width, which can limit the shrinkage.

3.5 X-ray Diffraction

Fig. 13 illustrates the XRD analysis of mortar with and without Al_2O_3 nanoparticles at 7 days of curing. Ettringite, portlandite, Alite and Belite were found to be major phases for the specimens. Changes in peak height and formation of new peaks were found at 7 days. Intensity of Alite and Belite phase decreased and a new peak of portlandite (2 theta of 16, 28 deg.) were found. However, no other new crystalline phase was found with nano-Al_2O_3 addition. The results indicate that, $Ca(OH)_2$ crystals (portlandite) which needs for formation of C-S-H gel appears in mortars containing nanoparticles, while for sample without nanoparticles, it is not appeared demonstrating synergic influence of nanoparticles on formation of subsequent C-S-H gel.

Conclusion

The following conclusions are drawn from the current study on mortars with incorporation of RHA, nano-Al_2O_3 and polypropylene fibers:

- The addition of RHA increased the 28-day compressive strength of samples up to 1% from their original level when cement was replaced by 10% RHA. Nevertheless addition of 20% and 30% RHA decreased compressive strength by up to 11% and 14%, respectively. However, this rate decreased at the age of 90 days.
- The addition of RHA reduced the 28-day flexural strength of samples up to 2%, 11%, and 14% from their original level when cement was replaced by 10%, 20% and 30% RHA. However, higher strength development was observed at 90 days when RHA content was increased from 10% to 30%. Incorporation of nano-Al_2O_3 enhanced the compressive and flexural strengths of samples containing 10% and 20% RHA. However, strength of the specimens containing 30% RHA enhanced when cement was replaced by 2% nano-Al_2O_3. The most advantageously effective amount of nano-Al_2O_3 was 3% by weight of the binder. For instance, the compressive strength increased up to 18% and 20% when 3% nano-Al_2O_3 was added to samples with 20% RHA at 28 and 90 days, respectively. Also, the 28-day and 90-day flexural strengths were enriched by up to 34% and 41% respectively, when 3% nano-Al_2O_3 was added to the samples with 10% RHA. Therefore, incorporation of nano-Al_2O_3 compensated the strength loss caused by 10% and 20% cement replacement by RHA. Furthermore, the strength development from 28 to 90 days was more in samples containing RHA at all levels.
- Water absorption of the specimens slightly decreased by the addition of 10% RHA and the values were same as that of the control sample with further increase of RHA up to 30%. Water absorption further decreased with the increase of nano-Al_2O_3 dosage up to 3%.

- Incorporation of polypropylene fiber enhanced the flexural strength of samples remarkably. The 28-day and 90-day flexural strengths increased by 18.6% and 23.1% respectively when 0.3% PPF was added to mixtures containing 10% RHA and 1% NA.
- SEM images confirmed the formation of denser microstructure with nano-Al_2O_3 addition. The densification of the microstructure is attributed to the formation of additional CSH by the RHA and CASH by the Al_2O_3. The compact microstructure improved bonding of the fibres with the matrix, which improved the flexural strength of the mortar specimens.
- Presence of RHA and PPF in mortars, both separately and together reduced drying shrinkage. The positive interaction between polypropylene fibers and rice husk ash resulted in the lowest drying shrinkage of the fibrous mortars.

References

[1] The European Cement Association, CEMBUREAU, Activity Report 2013, www.cembureau.eu

[2] Gonc¸alves M.R.F. Thermal insulators made with rice husk ashes: Production and correlation between properties and microstructure, Construction and Building Materials, 2007;21:2059–2065

[3] Faiziev S, Synthesis of ceramic compounds utilizing woody waste materials and rice husk, Construction and Building Materials Materials Science Forum Vols. 437-438 (2003) pp 411-414 21 2059–2065.

[4] Basha E A, Hashim R, Mahmud H B and Muntohar A S, Stabilization of Residual Soil with RHA and Cement, Construction and Building Materials, 2005;19:6:448-453.

[5] Al-Khalaf, Moayad N., and Hana A. Yousif. "Use of rice husk ash in concrete." International Journal of Cement Composites and Lightweight Concrete 6, no. 4 (1984): 241-248.

[6] Nehdi, Moncef, J. Duquette, and A. El Damatty. "Performance of rice husk ash produced using a new technology as a mineral admixture in concrete." Cement and concrete research 33, no. 8 (2003): 1203-1210.

[7] Ismail, Muhammad Shoaib, and A. M. Waliuddin. "Effect of rice husk ash on high strength concrete." Construction and Building Materials 10, no. 7 (1996): 521-526.

[8] Mehta, Povindar K. "Properties of blended cements made from rice husk ash." In ACI Journal Proceedings, vol. 74, no. 9. ACI, 1977.

[9] Ganesan, K., K. Rajagopal, and K. Thangavel. "Rice husk ash blended cement: assessment of optimal level of replacement for strength and permeability properties of concrete." Construction and Building Materials 22, no. 8 (2008): 1675-1683.

[10] Torkaman, Javad, Alireza Ashori, and Ali Sadr Momtazi. "Using wood fiber waste, rice husk ash, and limestone powder waste as cement replacement materials for lightweight concrete blocks." Construction and Building Materials 50 (2014): 432-436

[11] Sharma, R. K. "Effect of substitution of cement with rice husk ash on compressive strength of concrete using plastic fibres and super plasticizer." KSCE Journal of Civil Engineering 18.7 (2014): 2138-2142.

[12] Madandoust, Rahmat, Malek Mohammad Ranjbar, Hamed Ahmadi Moghadam, and Seyed Yasin Mousavi. "Mechanical properties and durability assessment of rice husk ash concrete." Biosystems Engineering 110, no. 2 (2011): 144-152.

[13] Safiuddin, Md, J. S. West, and K. A. Soudki. "Flowing ability of self-consolidating concrete and its binder paste and mortar components incorporating rice husk ash." *Canadian Journal of Civil Engineering* 37, no. 3 (2010): 401-412.

[14] Safiuddin, Md, J. S. West, and K. A. Soudki. "Flowing ability of the mortars formulated from self-compacting concretes incorporating rice husk ash." *Construction and Building Materials* 25, no. 2 (2011): 973-978.

[15] Rößler, Christiane, Danh-Dai Bui, and Horst-Michael Ludwig. "Rice husk ash as both pozzolanic admixture and internal curing agent in ultra-high performance concrete." Cement and Concrete Composites 53 (2014): 270-278.

[16] Kishore, Ravande, V. Bhikshma, and P. Jeevana Prakash. "Study on strength characteristics of high strength rice husk ash concrete." Procedia Engineering 14 (2011): 2666-2672

[17] Memon, Shazim Ali, Muhammad Ali Shaikh, and Hassan Akbar. "Utilization of rice husk ash as viscosity modifying agent in self compacting concrete." Construction and building materials 25, no. 2 (2011): 1044-1048.

[18] Van Tuan, Nguyen, Guang Ye, Klaas Van Breugel, Alex LA Fraaij, and Danh Dai Bui. "The study of using rice husk ash to produce ultra high performance concrete" Construction and Building Materials 25, no. 4 (2011): 2030-2035.

[19] Madandoust, R., E. Mohseni, S.Y. Mousavi and M. Namnevis, 2015. An experimental investigation on the durability of self-compacting mortar containing nano-SiO_2, nano-Fe_2O_3 and nano-CuO. Construct. Build. Mater., 86: 44-50.

[20] Noorvand, Hassan, Abang Abdullah Abang Ali, Ramazan Demirboga, Nima Farzadnia, and Hossein Noorvand. "Incorporation of nano TiO_2 in black rice husk ash mortars." Construction and Building Materials 47 (2013): 1350-1361.

[21] Mohseni, E., M.M. Ranjbar, M.A. Yazdi, S.S. Hosseiny and E. Roshandel, The effects of silicon dioxide, iron(III) oxide and copper oxide nanomaterials on the properties of self-compacting mortar containing fly ash. Magaz. Concrete Res. 2015;67;20:1112-1124

[22] Yang, J., E. Mohseni, B. Behforouz and M.M. Khotbehsara, An experimental investigation into the effects of Cr_2O_3 and ZnO_2 nanoparticles on the mechanical properties and durability of self-compacting mortar, International Journal of Materials Research, 106;8;886-892.

[23] Khotbehsara M.M., Mohseni E, Yazdi M.A, Sarker P, and Ranjbar M.M, Effect of nano-CuO and fly ash on the properties of self-compacting mortar. Construct. Build. Mater., 2015;94:758-766.

[24] E. Mohseni, M.M. Ranjbar and K.D. Tsavdaridis, Durability Properties of High-Performance Concrete Incorporating Nano-TiO2 and Fly Ash, American Journal of Engineering and Applied Sciences 2015, 8;4:519.526.

[25] Bayasi, Ziad, and Jack Zeng. "Properties of polypropylene fiber reinforced concrete." *ACI Materials Journal* 90, no. 6 (1993).

[26] Bayasi, Ziad, and Jack Zeng. "Properties of polypropylene fiber reinforced concrete." *ACI Materials Journal* 90, no. 6 (1993).

[27] Mydin, Md Azree Othuman, and Sara Soleimanzadeh. "Effect of polypropylene fiber content on flexural strength of lightweight foamed concrete at ambient and elevated temperatures." Advances in Applied Science Research 3, no. 5 (2012): 2837-2846...

[28] Ramezanianpour, A. A., M. Esmaeili, S. A. Ghahari, and M. H. Najafi. "Laboratory study on the effect of polypropylene fiber on durability, and physical and mechanical characteristic of concrete for application in sleepers." Construction and Building Materials 44 (2013): 411-418

[29] Alhozaimy, A. M., P. Soroushian, and F. Mirza. "Mechanical properties of polypropylene fiber reinforced concrete and the effects of pozzolanic materials." Cement and Concrete Composites 18, no. 2 (1996): 85-92.

[30] Flores Medina, N., G. Barluenga, and F. Hernández-Olivares. "Enhancement of durability of concrete composites containing natural pozzolans blended cement

through the use of Polypropylene fibers." Composites Part B: Engineering 61 (2014): 214-221.

[31] Bagherzadeh, Roohollah, et al. "An investigation on adding polypropylene fibers to reinforce lightweight cement composites (LWC)." journal of Engineered Fibers and Fabrics 7.4 (2012): 13-21.

[32] Salas, Andres, et al. "Comparison of two processes for treating rice husk ash for use in high performance concrete." Cement and concrete research 39.9 (2009): 773-778.

[33] ASTM C778-13 (2011) Standard Specification for Standard Sand, in: Annual Book of ASTM Standards, ASTM, Philadelphia, PA.

[34] ASTM C150 (2011): Standard specification for Portland cement, in: Annual Book of ASTM Standards, ASTM, Philadelphia, PA.

[35] ASTM C311 (2011) Standard Test Methods for Sampling and Testing Fly Ash or Natural Pozzolans for Use in Portland-Cement Concrete, in: Annual Book of ASTM Standards, ASTM, Philadelphia, PA.

[36] Nagataki, S., "Mineral admixtures in concrete: state of the art and trends" Proceedings of V. Mohan Malhotra Symposium on Concrete Technology: Past, Present, and Future, SP-144, P.K. Mehta, ed., American Concrete Institute, Farmington Hills, Michigan, USA, 1994, pp.447-482.

[37] Hwang, CL & Chandra, S., "The Use of Rice Husk Ash in Concrete", in S Chandra (ed.), Waste materials used in concrete manufacturing, William Andrew, 1997.

[38] ASTM C494 (2011) Standard Specification for Chemical Admixtures for Concrete, in: Annual Book of ASTM Standards, ASTM, Philadelphia, PA.

[39] Sobolev K, Nanomodification of cement, in: NSF Workshop on Nanomodification of Cementitious Materials, Portland Cement Concrete and Asphalt Concrete, Florida, USA, 2006.

[40] ASTM C305 (2011) Standard Practice for Mechanical Mixing of Hydraulic Cement Pastes and Mortars of Plastic Consistency, in: Annual Book of ASTM Standards, ASTM, Philadelphia, PA.

[41] ASTM-C109 (2011) Standard Test Method for Compressive Strength of Hydraulic Cement Mortars (using 50 mm [2 in.] Cube Specimens), in: Annual Book of ASTM Standards, ASTM, Philadelphia, PA.

[42] ASTM C157/C157M (2003) Standard Test Method for Length Change of Hardened Hydraulic Cement Mortar and Concrete, in: Annual Book of ASTM Standards, ASTM, Philadelphia, PA.

[43] ASTM C490-00a (2003) Standard Practice for Use of Apparatus for Determination of Length Change of Hardened Cement Paste, in: Annual Book of ASTM Standards, ASTM, Philadelphia, PA.

[44] Zerbino, R., G. Giaccio, and G. C. Isaia. "Concrete incorporating rice-husk ash without processing." Construction and building materials 25, no. 1 (2011): 371-378.

[45] A.L.G. Gastaldini, G.C. Isaia, T.F. Hoppe, F. Missau, A.P. Saciloto, Influence of the use of rice husk ash on the electrical resistivity of concrete: A technical and economic feasibility study, Construction and Building Materials 2009; 23:3411–3419.

[46] Mohseni, E., B.M. Miyandehi, J. Yang and M.A. Yazdi, 2015. Single and combined effects of nano-SiO_2, nano-Al_2O_3 and nano-TiO_2 on the mechanical, rheological and durability properties of self-compacting mortar containing fly ash. Construct. Build. Mater., 84: 331-340.

[47] Chao-Lung, Hwang, Bui Le Anh-Tuan, and Chen Chun-Tsun. "Effect of rice husk ash on the strength and durability characteristics of concrete." Construction and building materials 25, no. 9 (2011): 3768-3772.

[48] Hall C (1989) Water sorptivity of mortars and concretes: a review. Mag Concr Res 41(147):51–61.

[49] Malhotra VM, Caretta AGG, Bilodeau A. Mechanical properties and durability of polypropylene fiber reinforced high-volume fly ash concrete for shotcrete applications. ACI Mater J 1994;91:478–86.

[50] Liu L-F, Wang P-M, Yang X-J. Effect of polypropylene fiber on dry-shrinkage ratio of cement mortar. Jianzhu Cailiao Xuebao J Build Mater 2005;8:373–7.

[51] Salih SA, Al-Azaawee ME. Effect of polypropylene fibers on properties of mortar containing crushed bricks as aggregate. Eng Technol 2008;26:1508–23.

[52] Kırca O, Sahin M. The influence of using polypropylene fiber on durability of white concrete. In: 5th National concrete congress, durability of concrete, Istanbul; 2003: 375–82.

Table 1: Chemical composition and physical properties of cement and RHA

	Constituents (wt.%)	Cement	RHA
Chemical composition	SiO_2	21.75	91.15
	Al_2O_3	5.15	0.41
	Fe_2O_3	3.23	0.21
	CaO	63.75	0.41
	MgO	1.15	0.45
	SO_3	1.95	0.62
	K_2O	0.56	6.25
	Na_2O	0.33	0.05
	L.O.I	2.08	0.45
Physical properties	Surface area (cm^2/g)	3105	4091
	Specific gravity (g/cm^3)	3.15	2.07

Table 2: Properties of polypropylene fiber

Unit weight (g/cm^3)	0.9-0.91
Reaction with water	Hydrophobic
Tensile strength (MPa)	300-400
Elongation at break (%)	100-600
Melting point (◦C)	175
Thermal conductivity (W/m/K)	0.12
Length (mm)	6
Diameter (μm)	20

606

Table 3: Mix details of mortars 607

Sample ID	Cement (kg/m^3)	RHA (kg/m^3)	NA (kg/m^3)	PPF (kg/m^3)	Water (kg/m^3)	Sand (kg/m^3)	SP (kg/m^3)
CO	450	0	0	0	220	1430	0.9
RHA10	405	45	0	0	220	1415	1.8
RHA10NA1	400.5	45	4.5	0	220	1410	1.8
RHA10NA2	396	45	9	0	220	1400	1.8
RHA10NA3	391.5	45	13.5	0	220	1395	1.8
RHA20	360	90	0	0	220	1400	2.25
RHA20NA1	355.5	90	4.5	0	220	1390	2.25
RHA20NA2	351	90	9	0	220	1385	2.25
RHA20NA3	346.5	90	13.5	0	220	1380	2.25
RHA30	315	135	0	0	220	1380	3.25
RHA30NA1	310.5	135	4.5	0	220	1375	3.25
RHA30NA2	306	135	9	0	220	1370	3.25
RHA30NA3	301.5	135	13.5	0	220	1360	3.25
PP0.3	450	0	0	2.7	220	1430	1.5
RHA10PP0.3	405	45	0	2.7	220	1415	2.25
RHA10NA1PP0.3	400.5	45	4.5	2.7	220	1410	2.25
RHA10NA2PP0.3	396	45	9	2.7	220	1400	2.25
RHA10NA3PP0.3	391.5	45	13.5	2.7	220	1395	2.25
RHA20PP0.3	360	90	0	2.7	220	1400	3.25
RHA20NA1PP0.3	355.5	90	4.5	2.7	220	1390	3.25
RHA20NA2PP0.3	351	90	9	2.7	220	1385	3.25
RHA20NA3PP0.3	346.5	90	13.5	2.7	220	1380	3.25
RHA30PP0.3	315	135	0	2.7	220	1380	4.5
RHA30NA1PP0.3	310.5	135	4.5	2.7	220	1375	4.5
RHA30NA2PP0.3	306	135	9	2.7	220	1370	4.5
RHA30NA3PP0.3	301.5	135	13.5	2.7	220	1360	4.5

608

609

610

611

612

613

Table 4: Compressive strength of mortars

Sample ID	Compressive strength (MPa)			
	28 days	% of increase or decrease	90 days	% of increase or decrease
CO	45.1		50.2	
RHA10	45.3	0.44	50.3	0.2
RHA10NA1	45.6	1.11	51.1	1.8
RHA10NA2	50.3	11.5	57	13.5
RHA10NA3	52.6	16.6	59.6	18.7
RHA20	40.1	-11.1	45.7	-9.0
RHA20NA1	41.6	-7.7	47.3	-5.8
RHA20NA2	43.2	-4.2	49.1	-2.2
RHA20NA3	46.7	3.5	53.1	5.8
RHA30	38.7	-14.2	44.1	-12.1
RHA30NA1	40.1	-11.1	45.7	-9.0
RHA30NA2	40.3	-10.6	45.9	-8.6
RHA30NA3	39.6	-12.2	45.3	-9.8
PP0.3	46.9	4.0	53.4	6.4
RHA10PP0.3	45.4	0.6	51.9	3.4
RHA10NA1PP0.3	47.2	4.7	53.4	6.4
RHA10NA2PP0.3	51.6	14.4	58.4	16.3
RHA10NA3PP0.3	53.3	18.2	60.3	20.1
RHA20PP0.3	41.6	-7.8	47.3	-5.8
RHA20NA1PP0.3	41.9	-7.1	47.5	-5.4
RHA20NA2PP0.3	42.9	-4.9	48.9	-2.6
RHA20NA3PP0.3	45.9	1.8	52.1	3.8
RHA30PP0.3	39.5	-12.4	45	-10.3
RHA30NA1PP0.3	40.2	-10.9	45.7	-9.0
RHA30NA2PP0.3	41.6	-7.8	47.3	-5.8
RHA30NA3PP0.3	40.9	-9.3	46.3	-7.8

Table 5: Flexural strength of mortars

Sample ID	Flexural Strength (MPa)			
	28 days	% of increase or decrease	90 days	% of increase or decrease
CO	6.76		7.78	
RHA10	6.64	-1.8	7.8	0.3
RHA10NA1	6.75	-0.1	7.92	1.8
RHA10NA2	7.55	11.6	8.84	13.6
RHA10NA3	7.89	16.7	9.24	18.8
RHA20	6.02	-10.9	7.08	-9.0
RHA20NA1	6.24	-7.7	7.33	-5.8
RHA20NA2	6.48	-4.1	7.61	-2.2
RHA20NA3	7.01	3.6	8.23	5.9
RHA30	5.81	-14.1	6.84	-12.1
RHA30NA1	6.02	-10.9	7.08	-9.0
RHA30NA2	6.05	-10.5	7.11	-8.6
RHA30NA3	5.94	-12.1	7.02	-9.8
PP0.3	7.97	17.9	9.72	24.9
RHA10PP0.3	7.72	14.2	9.44	21.3
RHA10NA1PP0.3	8.02	18.7	9.72	24.9
RHA10NA2PP0.3	8.77	29.7	10.63	36.6
RHA10NA3PP0.3	9.06	34.0	10.97	41
RHA20PP0.3	7.07	4.6	8.61	10.7
RHA20NA1PP0.3	7.12	5.3	8.65	11.2
RHA20NA2PP0.3	7.29	7.8	8.90	14.4
RHA20NA3PP0.3	7.80	15.4	9.48	21.8
RHA30PP0.3	6.72	-0.5	8.19	5.3
RHA30NA1PP0.3	6.83	1.0	8.32	6.9
RHA30NA2PP0.3	7.07	4.6	8.61	10.7
RHA30NA3PP0.3	6.95	2.8	8.43	8.4

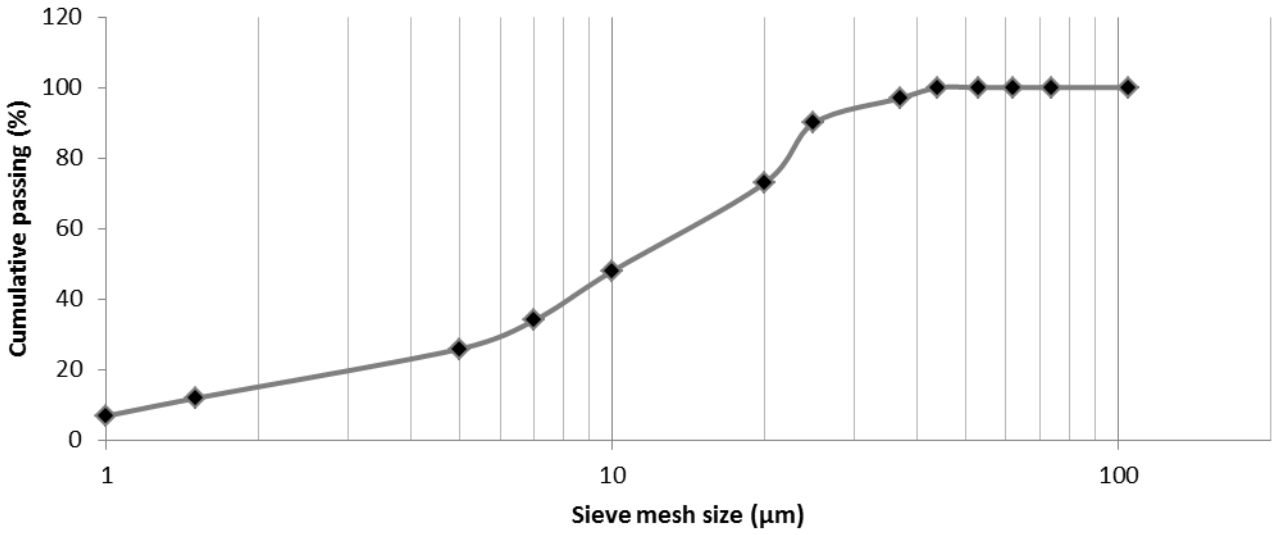

Fig. 1. Particle size distribution of RHA

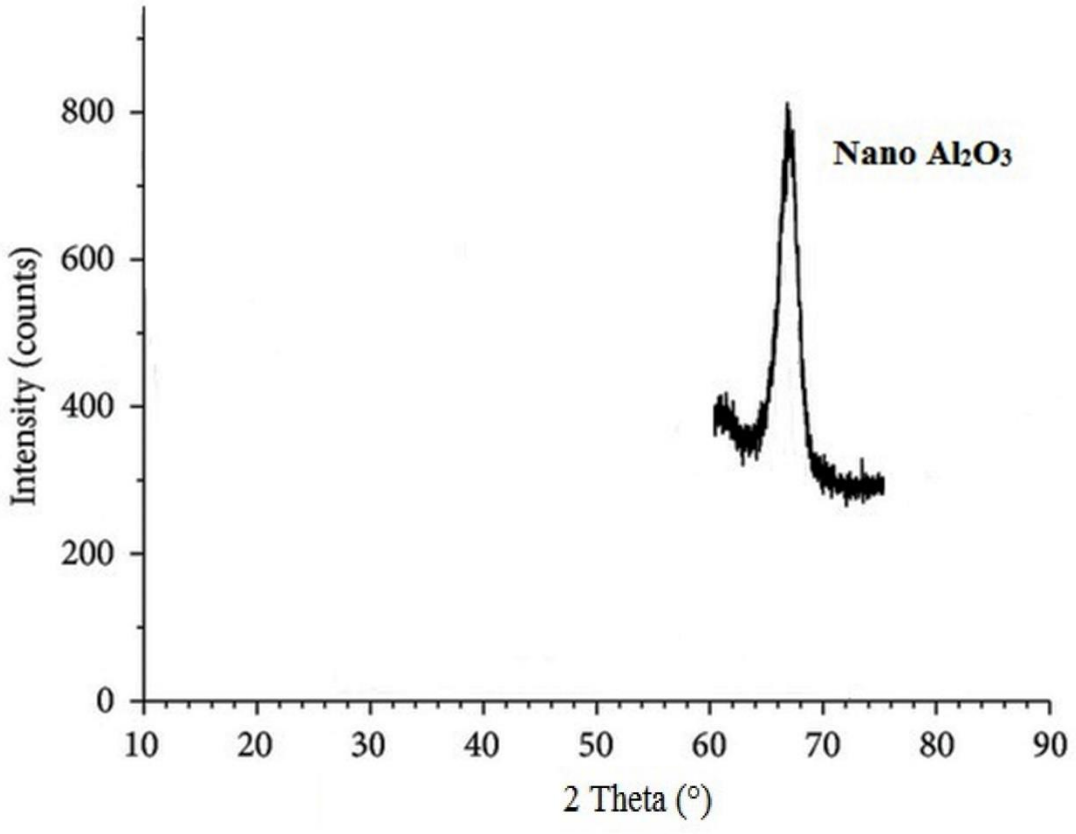

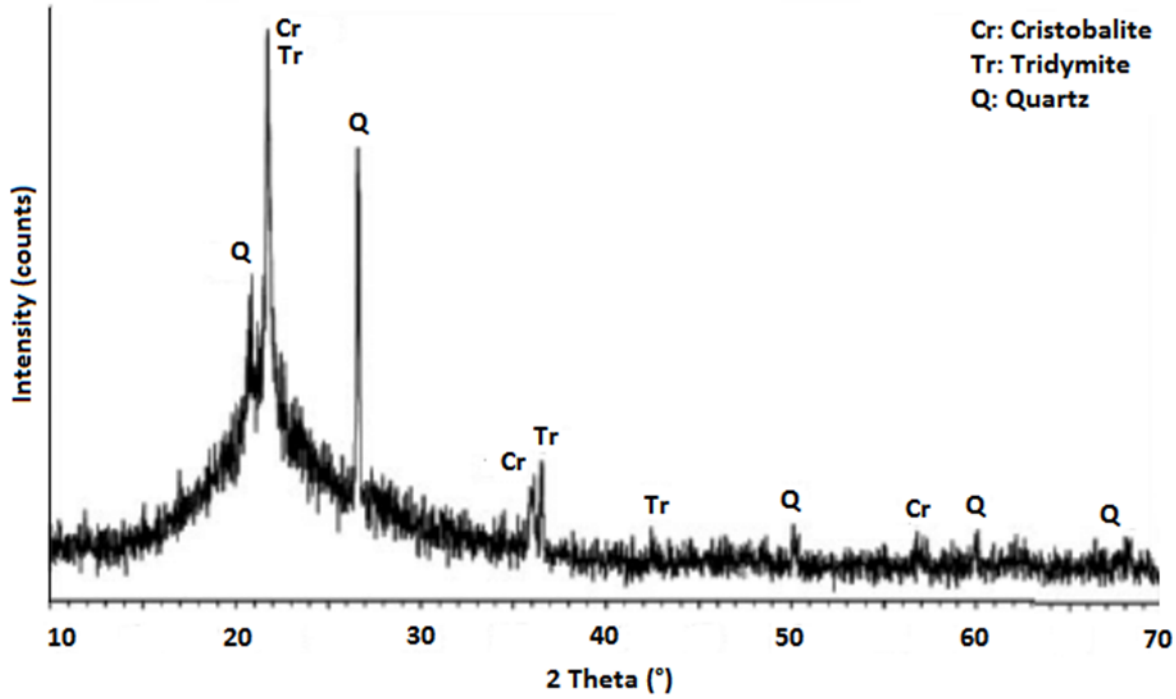

631

Fig. 2. XRD diagram of nano-Al_2O_3 (top) and RHA (bottom) 632

633

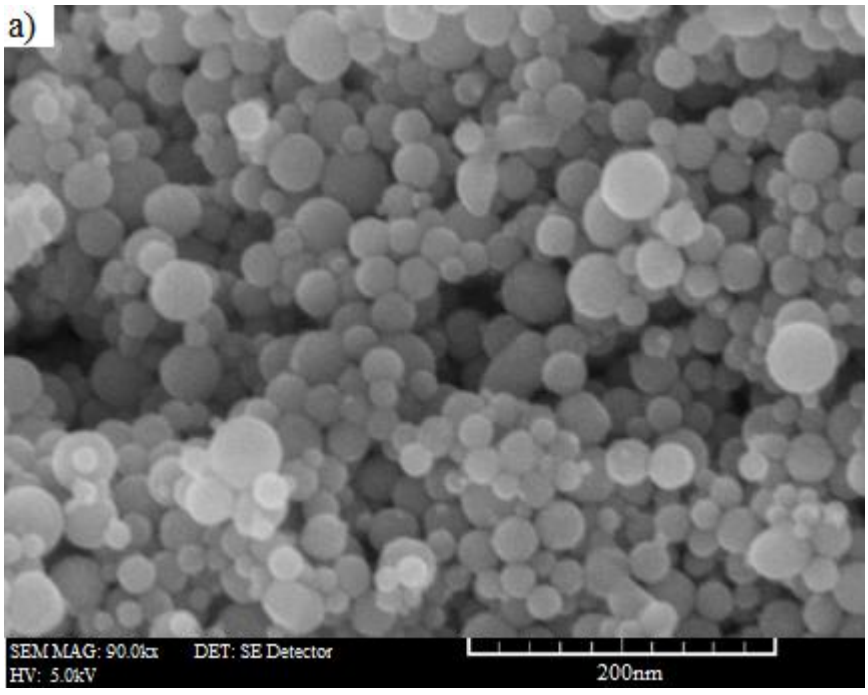

634

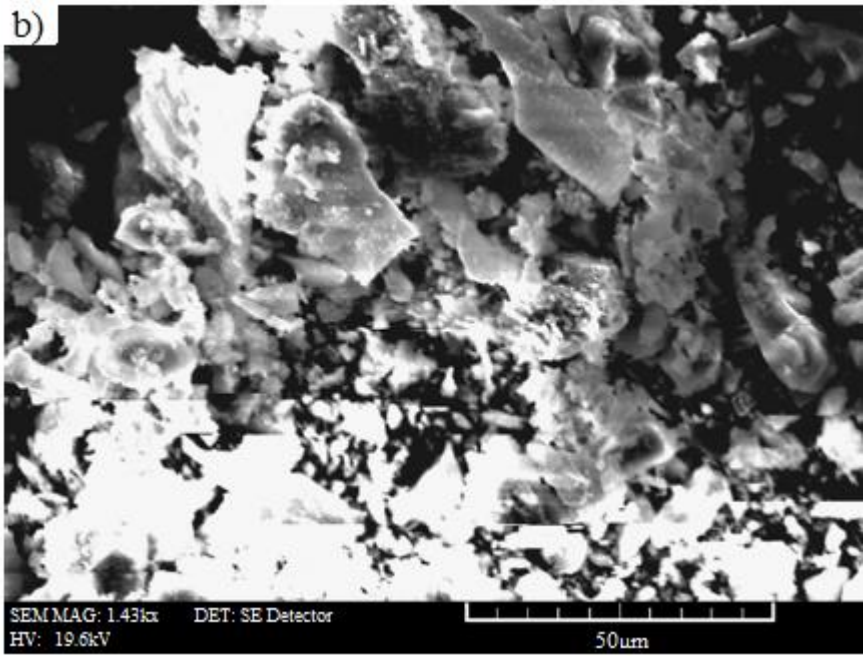

Fig. 3. SEM micrograph of the a) nano-Al_2O_3 and b) RHA

Fig. 4. Polypropylene fibers

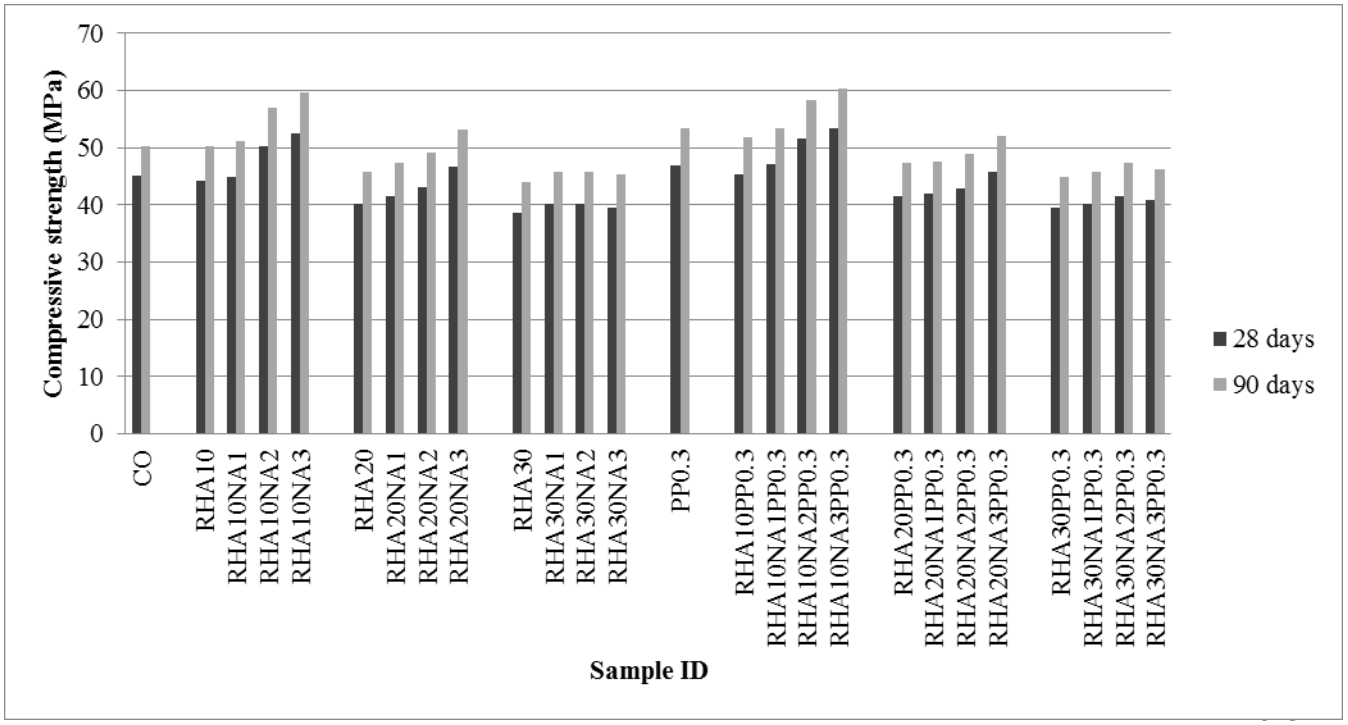

Fig. 5. Compressive strength values at 28 and 90 days of curing

646

647

648

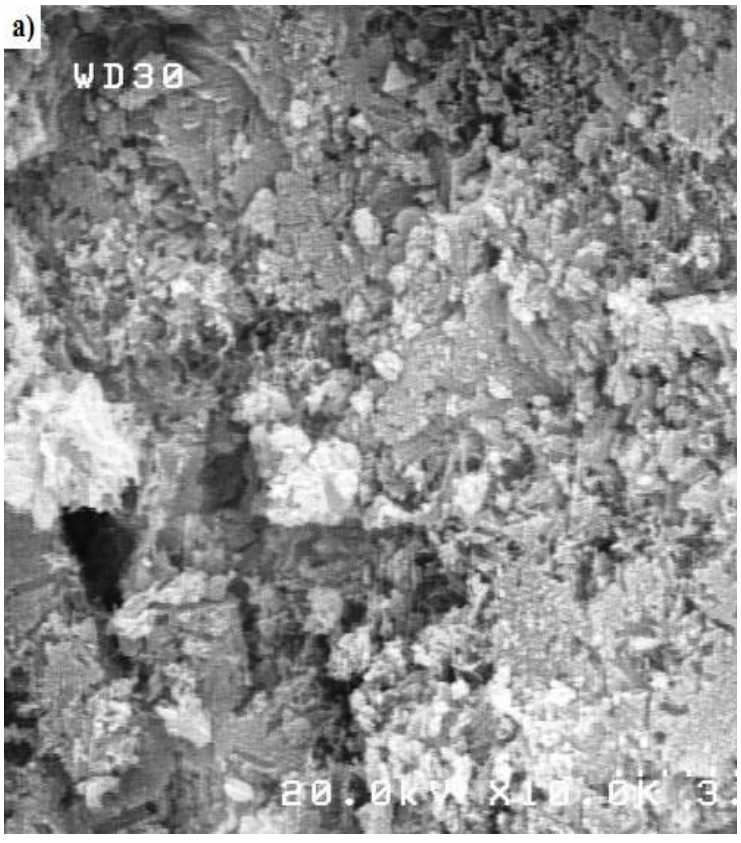

649

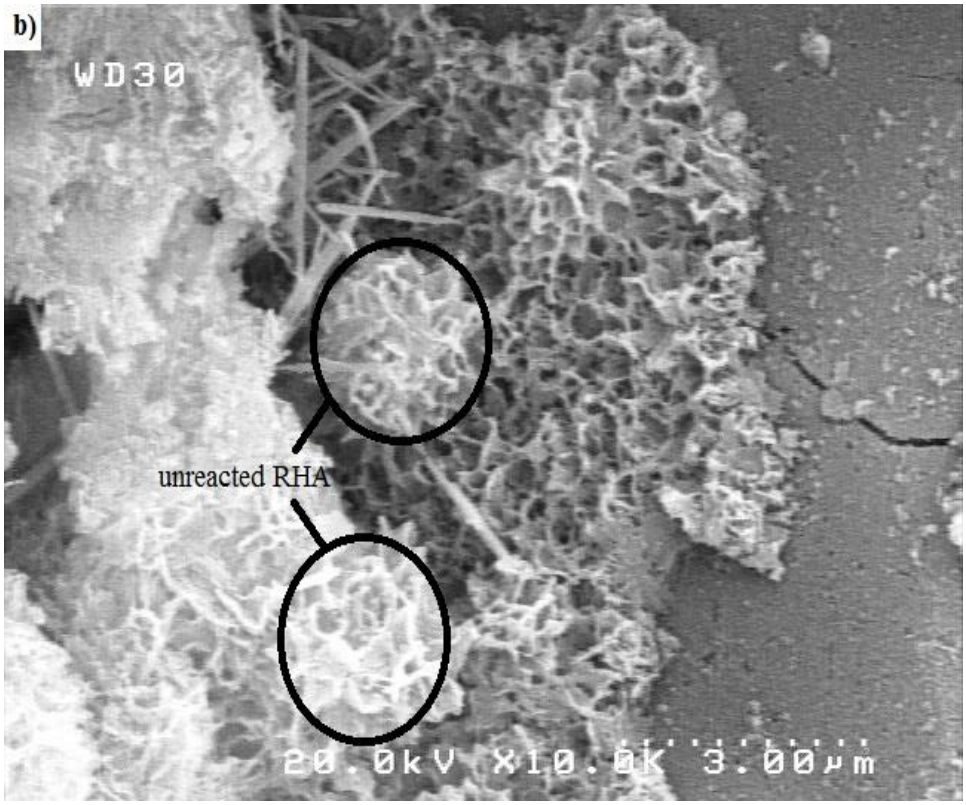

Fig. 6. SEM images of a) Control b) RHA10 and c) RHA10NA3 mixtures at 28 days of curing

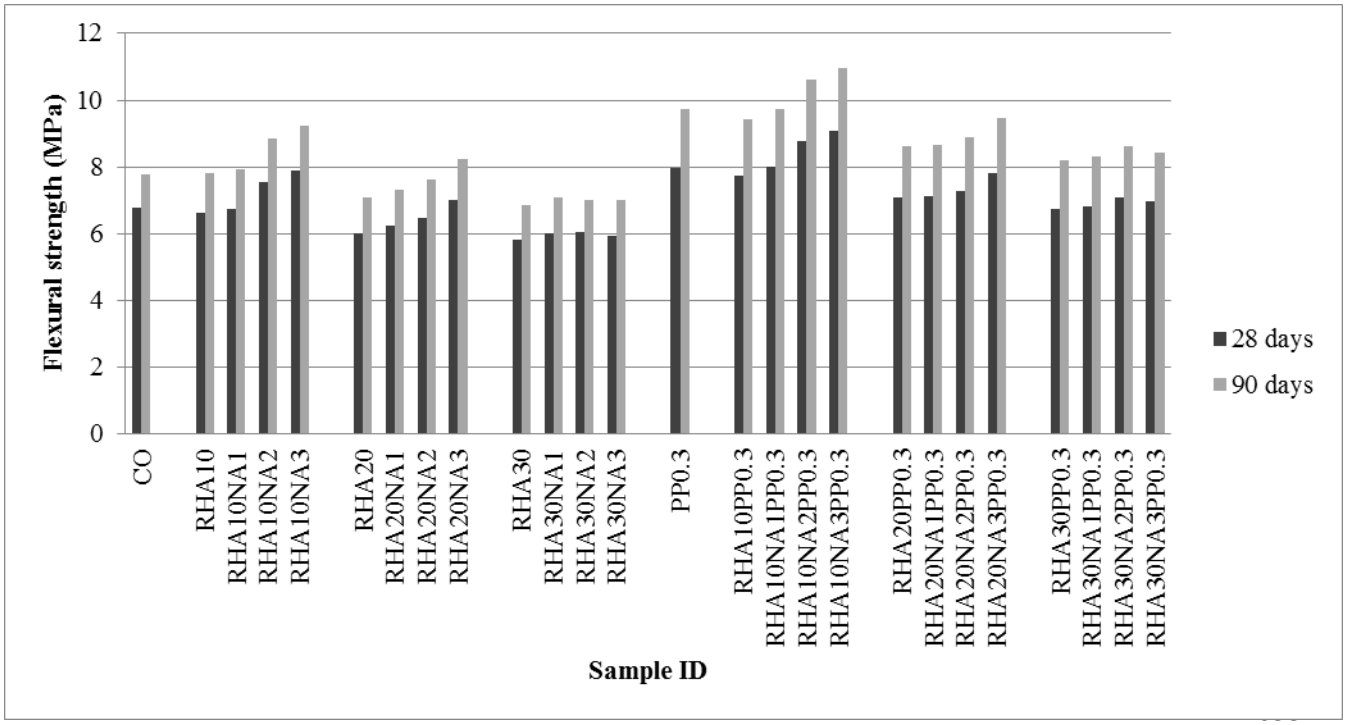

Fig. 7. Flexural strength values at 28 and 90 days of curing

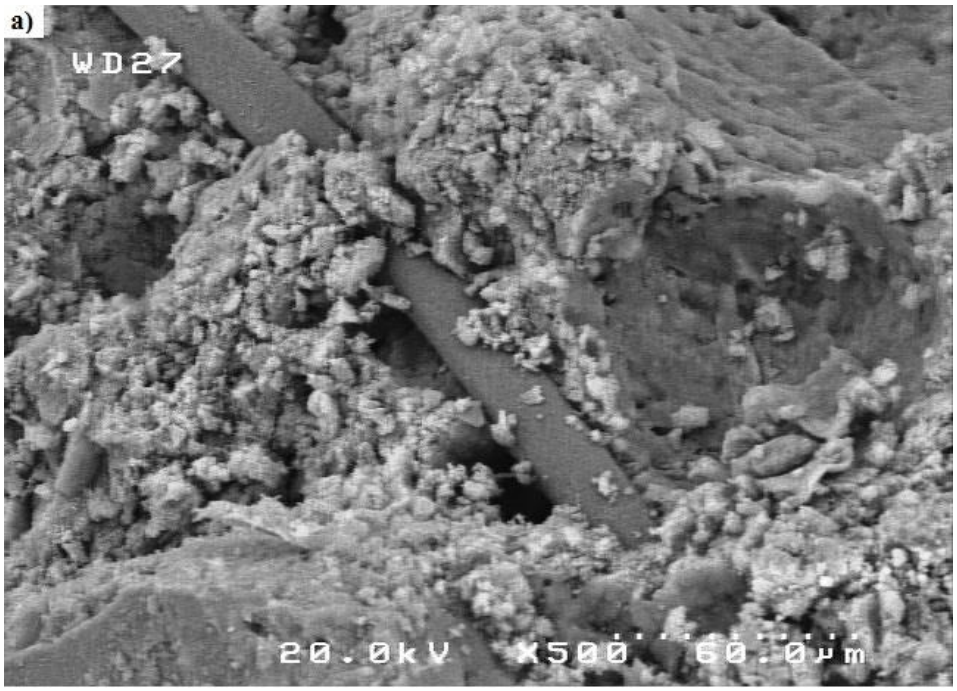

Fig. 8. SEM images of a) RHA10PPF0.3 and b) RHA10NA3PPF0.3 mixtures at 90 days of curing

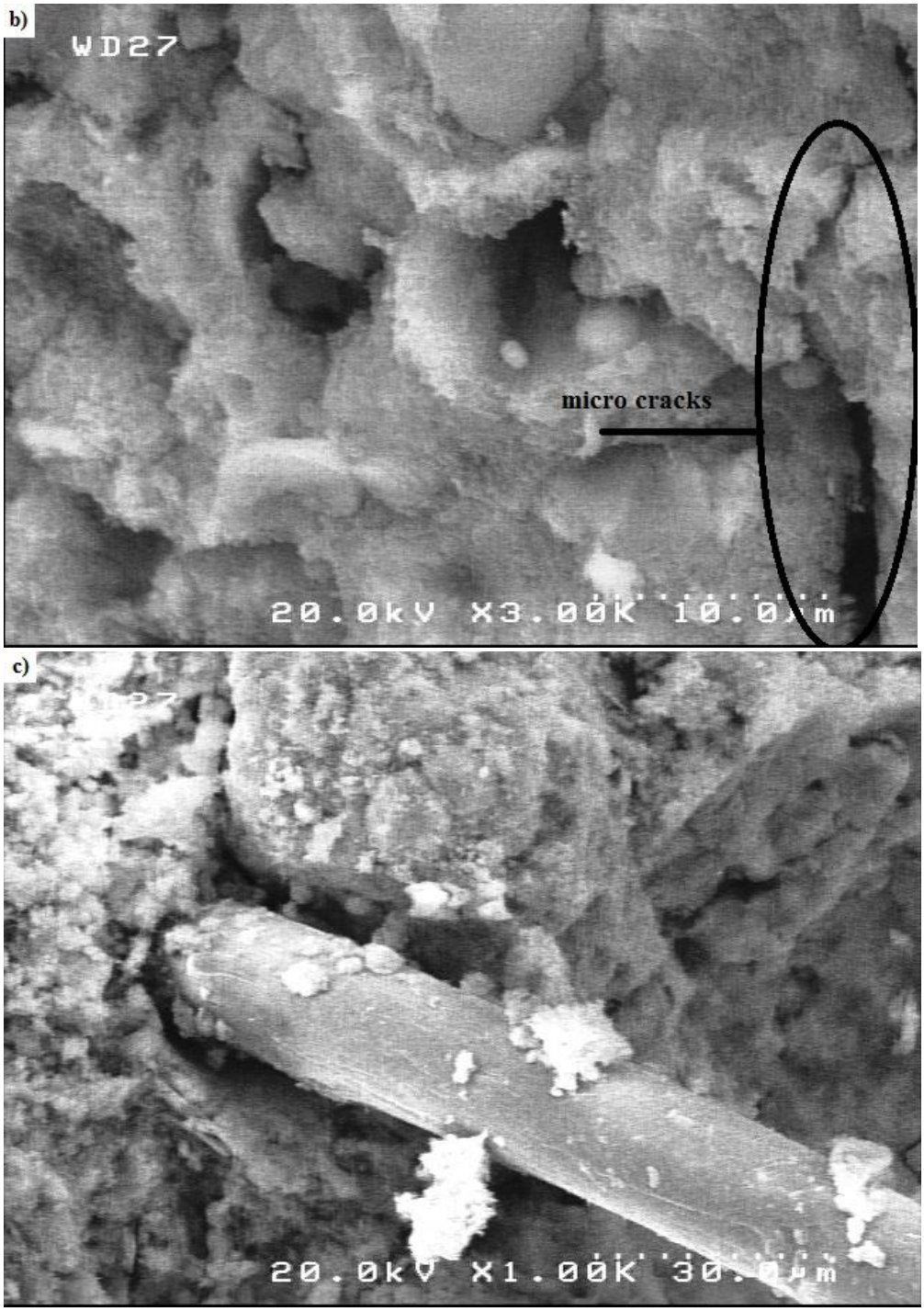

Fig. 9. SEM Micrograph of mortar fracture surface. (a) Control sample @ 15000 Res. b) Control sample @ 3000 Res. (c) Containing PPF @ 1000 Res at 90 days of curing

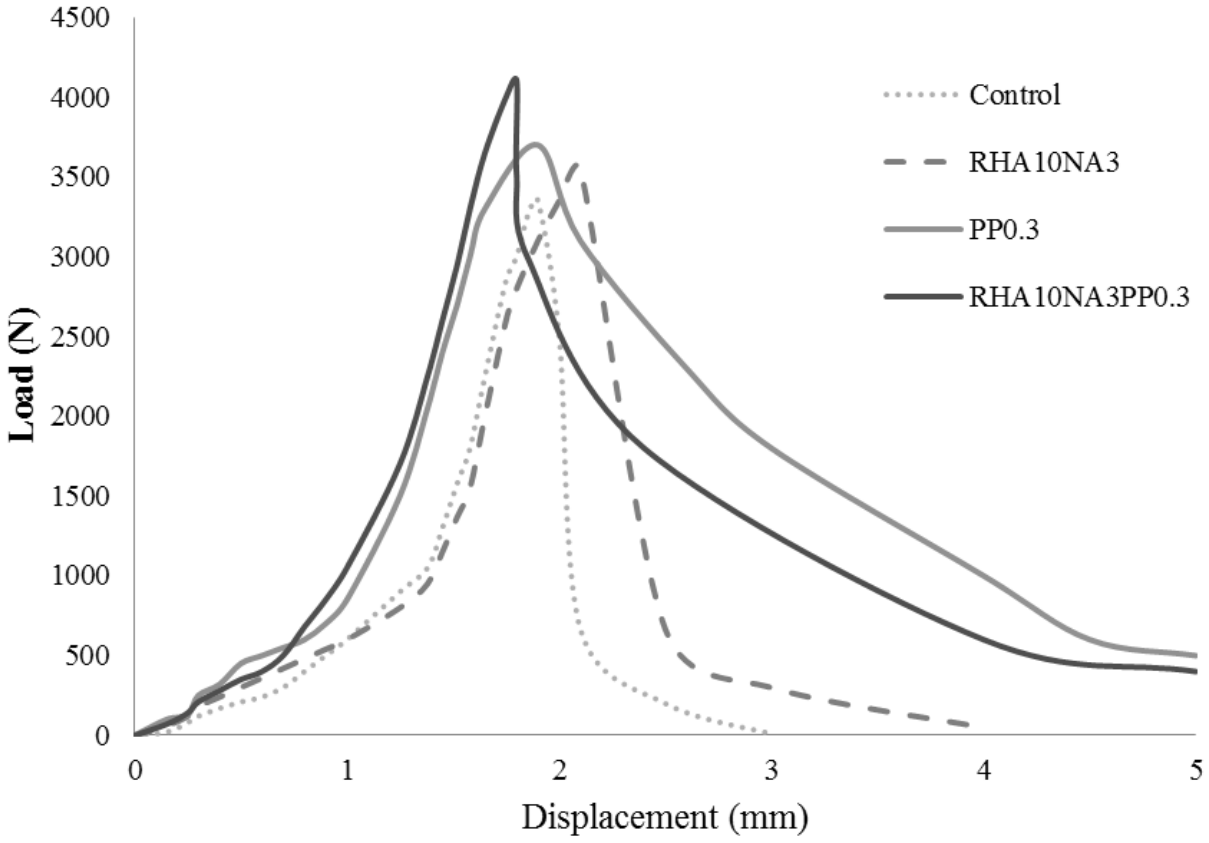

Fig. 10. Load-displacement curve for mortars reinforced with PPF at 90 days of curing.

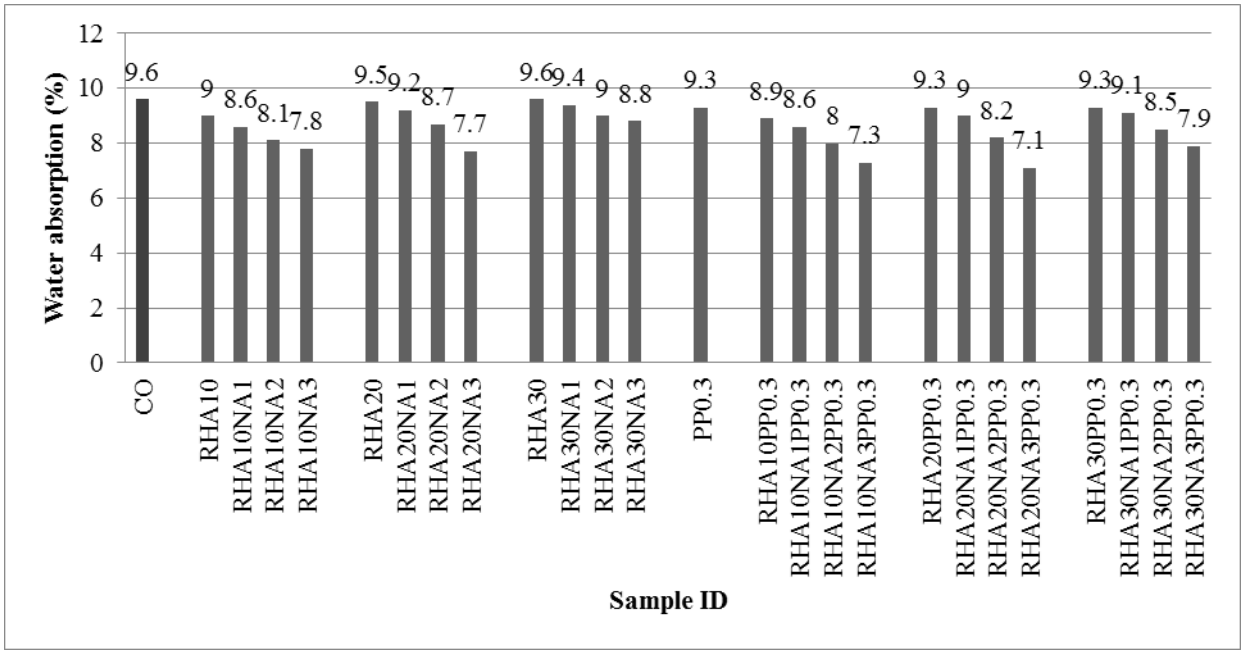

Fig. 11. Water absorption values at 28 days of curing

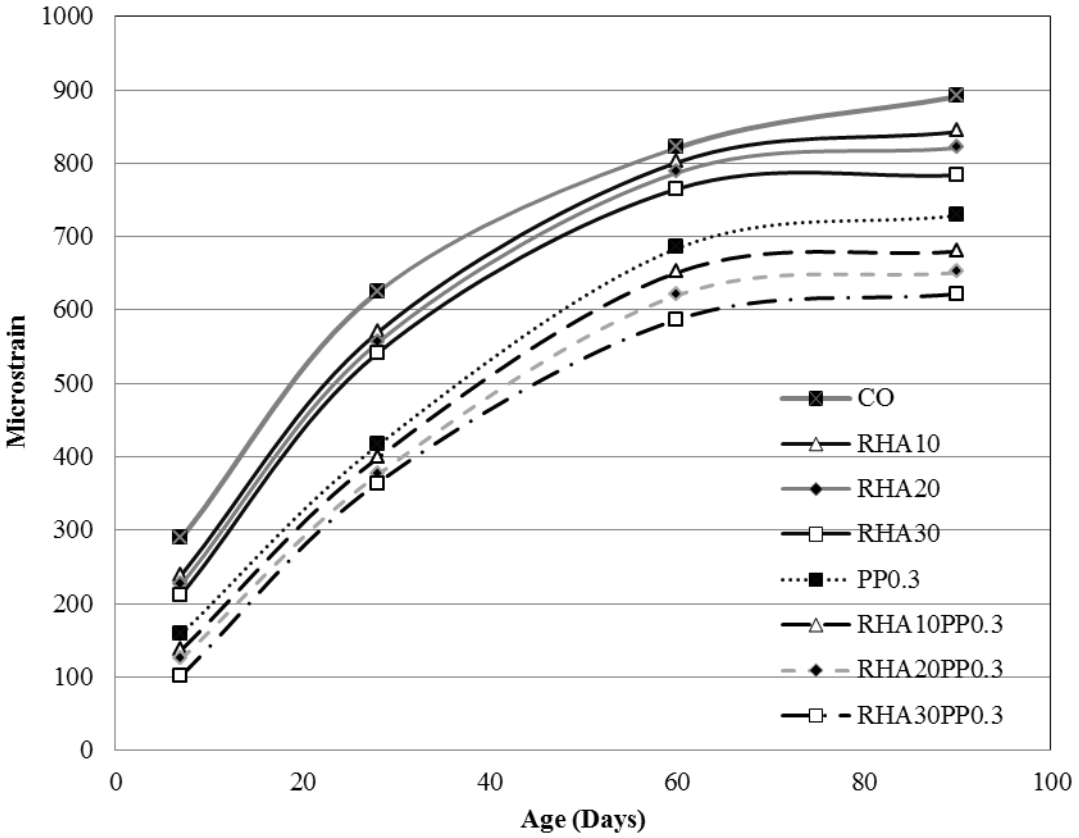

Fig. 12. Effect of RHA and polypropylene fibers on the drying shrinkage of mortars at various ages

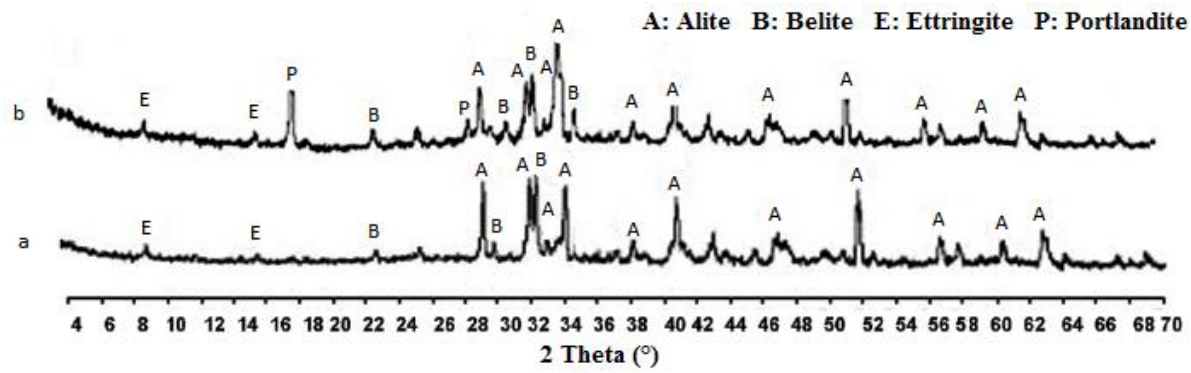

Fig. 13. XRD analysis of mortars a) without NA and b) with NA at 7 days of curing